Article

Not peer-reviewed version

Composites of Reduced Graphene Oxide Based on Silver Nanoparticles and Their Effect on Breast Cancer Stem Cells

Babu Vimalanathan , Devasena Thiyagarajan , Ruby Nirmala Mary , Magesh Sachidanandam , Savarimuthu Ignacimuthu , Dhanavathy Gnanasampanthapandian , Johnson Rajasingh *, Kanagaraj Palaniyandi *

Posted Date: 28 March 2025

doi: 10.20944/preprints202503.2185.v1

Keywords: Nanocomposites; Silver nanoparticles; Graphene oxide; Cancer stem cells; Raman spectroscopy; Mammosphere

 doi:10.20944/preprints202503.2185.v1

Article

Composites of Reduced Graphene Oxide Based on Silver Nanoparticles and Their Effect on Breast Cancer Stem Cells

Babu Vimalanathan [1], Devasena Thiyagarajan [2], Ruby Nirmala Mary [3], Magesh Sachidanandam [4], Savarimuthu Ignacimuthu [5], Dhanavathy Gnanasampanthapandian [7], Johnson Rajasingh [6,*] and Kanagaraj Palaniyandi [7,*]

[1] Crystal Growth Centre, Anna University, Chennai 600 025, Tamil Nadu, India
[2] Centre for Nanoscience and Nanotechnology, Anna University, Chennai 600 025, Tamil Nadu, India
[3] Department of Biotechnology, Periyar Maniammai Institute of Science and Technology, Thanjavur 613403, Tamil Nadu, India
[4] Department of Virology, King Institute of Preventive Medicine and Research, Chennai 600 032, Tamil Nadu, India
[5] Xavier Research Foundation, St Xavier's College, Palayamkottai 627002, Tamil Nadu, India
[6] Department of Bioscience Research & Medicine-Cardiology, The University of Tennessee Health Science Center, Memphis, TN, United States
[7] Cancer Science Laboratory, Department of Biotechnology, SRM Institute of Science and Technology, Chennai 603203, Tamil Nadu, India
* Correspondence: rjohn186@uthsc.edu (J.R.); kanagarp@srmist.edu.in (K.P.)

Abstract: Graphene and its related nanocomposites have garnered significant interest due to their distinct physiochemical and biological properties. In this study, reduced graphene-oxide-silver hybrid nanostructures were synthesized for applications in biomedical nanotechnology, particularly in targeting cancer stem cells (CSCs). A range of analytical techniques, such as X-ray diffraction (XRD), Raman spectroscopy, Fourier-transform infrared spectroscopy (FTIR), scanning electron microscopy (SEM), and UV-visible absorption spectroscopy (UV-VIS), were employed to characterize graphene oxide (GO), reduced graphene oxide (rGO)-silver nanoparticles (AgNPs) and their composite structures. The GO-rGO-AgNPs exhibited potent anticancer properties as evidenced by cell culture assays, spheroid formation assay, and quantitative RT-PCR analysis. Treatment of breast cancer cells (MCF-7) with GO, rGO, and AgNPs significantly reduced cell proliferation and mammosphere formation. Furthermore, these treatments downregulated the expression of marker genes associated with CSCs in MCF-7 cells. Among the tested materials, rGO-AgNP, sodium citrate-mediated GO-AgNP, and rGO-AgNP nanocomposites demonstrated superior inhibitory effects on cell survival compared to GO alone. These findings suggest that these nanocomposites hold promise as effective and non-toxic therapeutic agents for targeting cancer cells and CSCs, thereby offering a novel approach to cancer treatment.

Keywords: Nanocomposites; Silver nanoparticles; Graphene oxide; Cancer stem cells; Raman spectroscopy; Mammosphere

1. Introduction

Graphene, a single layer of sp2-hybridized carbon atoms arranged in a two-dimensional honeycomb lattice, has drawn significant attention in scientific and industrial applications due to its exceptional properties [1–4]. These include remarkable mechanical strength, high electron mobility, superior electronic transport, and excellent electrical conductivity. As a result, graphene has found applications in nanocomposites [5,6], nanoelectronics [7,8], and energy storage devices [9,10]. In

 doi:10.20944/preprints202503.2185.v1

addition, graphene nanoparticles have recently been increasingly explored for biological applications [11,12], such as drug delivery [13,14], cellular imaging, antibacterial activity [15–17], biosensing [18,19], and anticancer therapies [20–25].

Graphene oxide (GO), a hydrophilic derivative of graphene, produces stable and homogeneous, colloidal suspensions in aqueous and polar solvents due to its oxygen-containing functional groups. It serves as a precursor for reduced GO (rGO) through chemical deoxygenation [7,8]. With its large surface area, abundant functional groups, and high water solubility, GO has demonstrated potential in numerous biomedical applications, including drug delivery, biosensing, antibacterial, antiplatelet activity, anticancer therapies, and scaffolding for tissue engineering [26,27]. Notably, graphene materials can enhance cell adhesion, stimulate cell proliferation and promote differentiation, serving as effective scaffolds in regenerative medicine [26,28].

Graphene substrates have been shown to promote neurite outgrowth in mouse hippocampal cells, whereas rGO sheets induce neurite genesis of PC12 cells [28,29]. GO suspensions further promote the differentiation of mice embryonic stem (ES) cells and the osteogenic differentiation of human mesenchymal stem cells (MSCs) [30,31]. Beyond graphene, silver nanoparticles (AgNPs) have also been extensively studied due to their unique properties, including high surface areas and nanoscale dimensions. These characteristics make AgNPs useful in energy science, optics, electronics, catalysis, nanobiotechnology, and nanomedicine, especially as antibacterial agents [32,33]. Several studies have shown that AgNPs act as anti-angiogenic and anticancer agents in retinal endothelial cells [34]. AgNP treatment had significant effects on cytotoxicity observed in human lung fibroblasts (IMR-90), human glioblastoma cells (U251), and endothelial cells [35,36].

The combination of GO with AgNPs has gained significant interest because of the complementary and enhanced properties of these materials [37–39]. GO sheets provide a stable platform for the controlled binding and release of AgNPs, resulting in improved antibacterial and anticancer activities [40–42]. This synergy is particularly relevant for developing innovative therapeutic agents targeting multiple factors that contributed to cancer progression, metastasis and resistance to conventional treatments [43,44].

Cancer therapy remains a significant challenge due to multidrug resistance (MDR) and the role of cancer stem cells (CSCs) in tumor recurrence and metastasis [45]. Nanoparticle-mediated drug delivery offers a promising approach to address these issues by precisely targeting cancer cells and minimizing side effects [46]. In this study, we synthesized and characterized GO and rGO–silver nanocomposites using sodium citrate and evaluated their potential cytotoxic effects on breast CSCs. This research aims to contribute to the development of novel therapeutic agents for overcoming the limitations of current cancer treatments.

2. Materials and Methods

2.1. Chemicals

Graphite powder, Laboratory grade Thiourea, NaOH, $KMnO_4$, anhydrous ethanol, 98% H_2SO_4, 36% HCl, and 30% hydrogen peroxide (H_2O_2) aqueous solution were procured from Sigma Aldrich, Mumbai; they were employed with no additional refinement. Trypsin, water-soluble tetrazolium salt (WST-8), Dimethyl sulfoxide (DMSO). Deionized water was used to prepare aqueous solutions. All reagents and chemicals were purchased from Sigma-Aldrich (St Louis, MO, USA). The breast cancer cell line MCF-7 was purchased from NCCS (Pune, India). DMEM cell culture media, trypsin–EDTA, and antibiotics were procured from HiMedia (Bangalore, India). MTT and cell culture grade DMSO were procured from Sigma-Aldrich (USA). Fetal bovine serum was purchased from Thermoscientific (USA). Ultra-low attachment plate and Mammocult media were purchased from Stem Cell Technologies (Canada). The total RNA isolation (RNAeasy mini) kit and the DNAase kit were obtained from Qiagen (Germany). The SYBR master mix was procured from Promega (USA).

2.2. Preparation of Silver Nanoparticles

 doi:10.20944/preprints202503.2185.v1

AgNP synthesis was performed according to a procedure that has been documented previously [47]. In brief, AgNPs were synthesized by soaking 7.5 mM sodium citrate (1.10 g) in 500 mL water (Sigma-Aldrich) containing 5 mM $AgNO_3$ (0.424 g) for 12 h at 60°C. The production of AgNPs in the reaction mixture was responsible for the color shift from colorless to black. The reduction of the silver ions was monitored spectrophotometrically at 420 nm. Further characterization of the synthesized silver nanoparticles were performed as described previously [48].

2.3. Preparation of Graphene Oxide (GO) Sheets

Graphene oxide was produced by the modified Hummers method [49]. Graphite powder (1g) was mixed in 90 ml of 98% concentrated sulfuric acid. The mixture was stirred in ice bath for 30 min (10°C). Further 6g of $KMNO_4$ was added and stirred in ice bath for 18-24 h murky brown color paste was obtained (10°C), Later 500ml deionized water was added and stirred for 1h at 10°C. Following to this, 5ml of 30% H_2O_2 was added., mixed and stirred well using magnetic stirrer overnight in an ice bath. The hue shifted from murky brown to dark brown. Then, 200 ml of diluted HCl (HCl 1:10 H_2O) was added, mixed well for 30 minutes using magnetic stirrer. The color became yellowish brown. This was centrifuged at room temperature at 5000 rpm for 5 minutes. The pellet was allowed to settle down. The pellet was washed more than 5 times with de-ionized water to remove any residual ions. The graphene oxide pellet was suspended in 50 ml of de-ionized water and sonicated for 30 min. The sonicated graphene oxide nanosheets solution was dried at 60°C for 24 h in vacuum oven.

2.4. Preparation of rGO via Thermal Reduction

The GO was heated in an N_2 environment (flow rate of 0.12 m^3/h) in an oven at 750°C and then at 950°C to achieve thermal reduction. The GO was maintained at this temperature for 45 s [48,49] after reaching the target temperature.

2.5. Preparation of GO-Ag Nanocomposite

The silver-containing solution, which included $AgNO_3$ (5 mM, 200 mL) and sodium citrate (7.5 mM, 200 mL), was mixed with 0.5 g of GO powder. After the mixture was finalized, the solution was treated with pulsed microwave-assisted (MA) synthesis. To ensure the development of silver seeds deposited on the GO surface, the solution was placed in a microwave oven (Tatung Co., Taipei City, Taiwan; 900 W, 2.45 GHz) at 160°C for 5 min. After preparation, the GO–Ag solution was dried overnight at 60°C in a vacuum oven [50].

2.6. Preparation of rGO-Ag Nanocomposite

The silver-containing solution, which contained $AgNO_3$ (5 mM, 200 mL) and sodium citrate (7.5 mM, 200 mL), was mixed with 0.5 g of rGO powder. After the mixture was finalized, the solution was treated with pulse MA synthesis. To ensure the development of silver seeds deposited on the GO surface, the solution was placed in a microwave oven (Tatung Co., Taipei City, Taiwan; 900 W, 2.45 GHz) at 160°C for 5 min. After preparation, the rGO-Ag solution was dried all night at 60°C in a vacuum oven [42].

2.7. Characterization of Nanocomposites

The previously mentioned techniques were used to characterize GO, rGO, and the rGO–Ag nanocomposites [51]. The ultraviolet-visible (UV-Vis) spectra GO, rGO, and rGO–Ag were recorded by using an OPTIZEN POP-V spectrophotometer (Mecasys Co., Seoul, Republic of Korea). XRD measurements were performed with a Rigaku Ultima IV using CuKα radiation at a wavelength of 1.54 Å and a 10 mm Cu target slit. Raman spectral measurements were performed by using a Renishaw PLC Raman spectrometer at an excitation wavelength of 514 nm (argon ion laser source).

 doi:10.20944/preprints202503.2185.v1

The materials were dried and powdered with KBr pellets and examined with a Bruker Tensor 37 for FTIR analysis. Random micrographs were taken with an accelerating voltage of 15 kV at different points on a clean glass slide to which a droplet of the nanoparticle solution was transferred for SEM (Carl Zeiss, Germany).

2.8. Cell Viability Assay

MCF-7 cells were cultured in DMEM supplemented with 10% fetal bovine serum and 1% penicillin and streptomycin in an atmosphere of 5% CO_2 at 37°C. The cell viability was assessed by using trypan blue exclusion method. MCF-7 cells (1×10^4) were plated in 96-well plates and incubated overnight for attachment. MCF-7 cells were treated with different concentrations (1, 10, and 50 μM) of nanoparticles (GO, rGO, AgNPs) and their combinations for 48 h. After 48 h, the nanoparticles were carefully removed, the MTT reagent was added and incubated for 3 h at 37°C in a CO_2 incubator. The MTT media were discarded, and the formazon crystals were dissolved in dimethyl sulfoxide. The plates were read at 570 nm in an ELISA plate reader (BioTek, USA).

2.9. Mammosphere Formation Assay

The mammospheroid assay technique was used as reported previously [52]. MCF-7 cells were transferred to single cell suspensions with trypsin. The cells (500 cells/well) were mixed in mammocult media and plated in an ultra-low attachment plate (12 wells). The MCF-7 cells were incubated overnight. Subsequently, the cells were treated with nanoparticles (GO, rGO, AgNPs) at a dose of 10 μM and allowed to form mammospheres for 7 days. The mammospheres were imaged in an inverted phase contrast microscope (EVOS M5000) and the number of spheroids was counted.

2.10. Quantitative RT-PCR

The MCF-7 cells were plated in 10 cm^2 Petri dish and allowed to grow approximately 70% confluence. MCF-7 cells were treated with the nanoparticles (GO, rGO, AgNPs) at 10 μM for 24 h. After treatment, the cells were trypsinized to obtain a cell pellet. The cell pellet was used to isolate total RNA (RNeasy mini kit, Qiagen, Germany). The total RNA was treated with the DNase kit from Invitrogen (USA). The total RNA (2 μg) was converted to cDNA using the cDNA synthesis kit according to the manufacturer's instructions (iScript, BioRad, USA). The template DNA was used at 95°C for hot-start, 62°C for annealing, and 60°C for extension (QauntStudio5, Thermoscientific, USA). A total of 35 cycles were repeated to amplify target genes, such as *CD24*, *CD44*, *ALDH1*, *SOX-2*, *NANOG*, *OCT-4*, *EPCAM*, *LGR5*, and β-actin. The delta-delta CT values were converted into differences between the nanoparticle-treated groups.

2.11. Statistical Analysis

All three independent experimental data were analyzed statistically by one way analysis of variance (ANOVA) by using IBM-SPSS.30 statistical software. $P<0.05$ considered to be statistically significant when compared with the control groups. In between groups also compared using Tukey HSD and Duncan test.

3. Results

3.1. UV-Vis Spectroscopy

GO, rGO, and AgNO3 were combined to prepare the nanocomposite, and sodium citrate was used as a stabilizing and reducing agent. The UV-Vis spectra of GO, rGO, and the GO-Ag rGO-Ag nanocomposite are shown in Figure 1a–d. At 230 and 292 nm, GO showed two distinct peaks representing the π–π* transitions of aromatic C–C bonds and the n–π* transitions of C=O bonds. The UV-visible spectra also confirmed the presence of GO-AgNPs. As shown in Figure 1, GO exhibited a typical peak at 230 nm corresponding to the aromatic C=C bond, whereas AgNPs associated with the

 doi:10.20944/preprints202503.2185.v1

graphene layer showed a typical characteristic peak at around 410 nm, consistent with the AgNP formulation and surface plasmon resonance phenomena. The evolution of the rGO–Ag nanocomposite and the concomitant decrease of rGO and $AgNO_3$ were demonstrated clearly by the disappearance of the characteristic peaks of rGO and the presence of a new band originating from AgNPs.

Figure 1

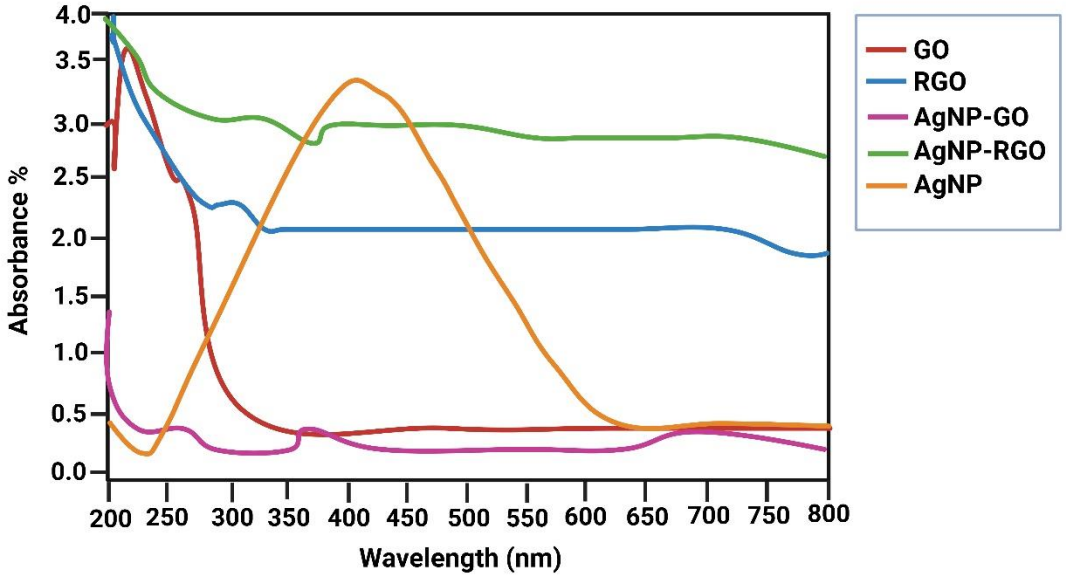

Figure 1. UV-Vis spectra of nanoparticles GO, rGO, AgNP-GO, AgNP-rGO and AgNP.

3.2. Powder X-Ray Diffraction (PXRD) Analysis

XRD was used to further demonstrate that GO and GO-AgNP are crystalline materials. The PXRD pattern of artificially generated GO, AgNPs, and GO-Ag nanocomposites is shown in Figure 2. The plane (001) was represented by a strong $2\theta = 10.19°$ value in the GO PXRD pattern. In addition, the (002) plane was reflected by a minor peak at $2\theta = 20.93°$. As oxygen-containing functional groups were added to graphite during its oxidation, the interlayer gap in GO increased compared to graphite.

However, as shown in Figure 2, a small variation in peak position towards a lower 2θ value confirmed the incorporation of AgNPs in GO sheets. From 2a and 2b, the peak at GO -10.9, GO-AgNP-10.8, 32.1 matching to the Figure 2e AgNP peak of 32.1 for comparison. Figure 2c and d the peak at rGO-25.4, Rgo-AgNP-25.4, 32.1 matching to the Figure 2e AgNP of 32.1 for comparison. However, in the rGO–Ag nanocomposites, in addition to the typical reflections of rGO (2θ=25.4°), two unique reflections appeared at 40.1° and 45.3° in the diffractogram, corresponding to the (111) and (200) planes, respectively. This shows that metallic AgNPs were formed during the reduction.

 doi:10.20944/preprints202503.2185.v1

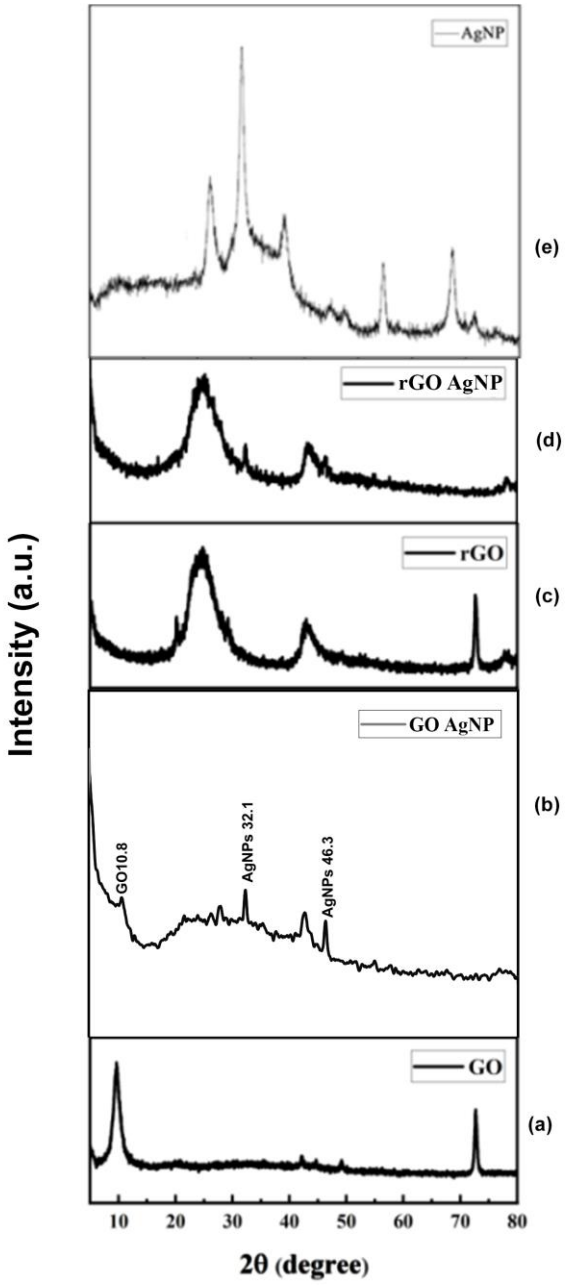

Figure 2. Powder XRD pattern of a. GO, b. GO-AgNP, c. rGO, d. rGO-AgNP, and e. AgNP composites.

3.3. SEM Analysis

The surface morphology of GO and the AgNP deposits on it were verified by using SEM. Stacking of the exfoliated nanosheets resulted in a well-packed, folded (and silky wave-like) morphology of the GO sheets. The surface morphology showed the appearance of a tightly folded curtain, with GO flakes overlapping instead of clumping. A remarkable morphological change was observed between GO and GO-AgNPs (Figure 3a–e). The AgNPs were uniformly dispersed on the surface of the composite nanosheets in distinct spherical shapes. The AgNPs appeared to be uniformly distributed over the GO sheets, as shown by the AgNPs distribution. Our results showed that the graphite exfoliated significantly during the oxidation process and that sodium citrate effectively reduced GO and $AgNO_3$ to GO-AgNPs (Figure 3).

 doi:10.20944/preprints202503.2185.v1

In contrast to GO, rGO showed flaky, scale-like layers or transparent, rippling, silk-like waves. Typical SEM images of the prepared rGO–Ag hybrids are shown in Figure 3. Well-dispersed AgNPs were deposited on the graphene. Curled and wavy morphology was exhibited when Ag crystallites were generated on graphene surfaces as spacers between neighboring sheets in AgNPs-doped rGO. As spacers keep adjacent sheets at a distance, the AgNPs were randomly distributed on the graphene sheets at a considerable distance from one another.

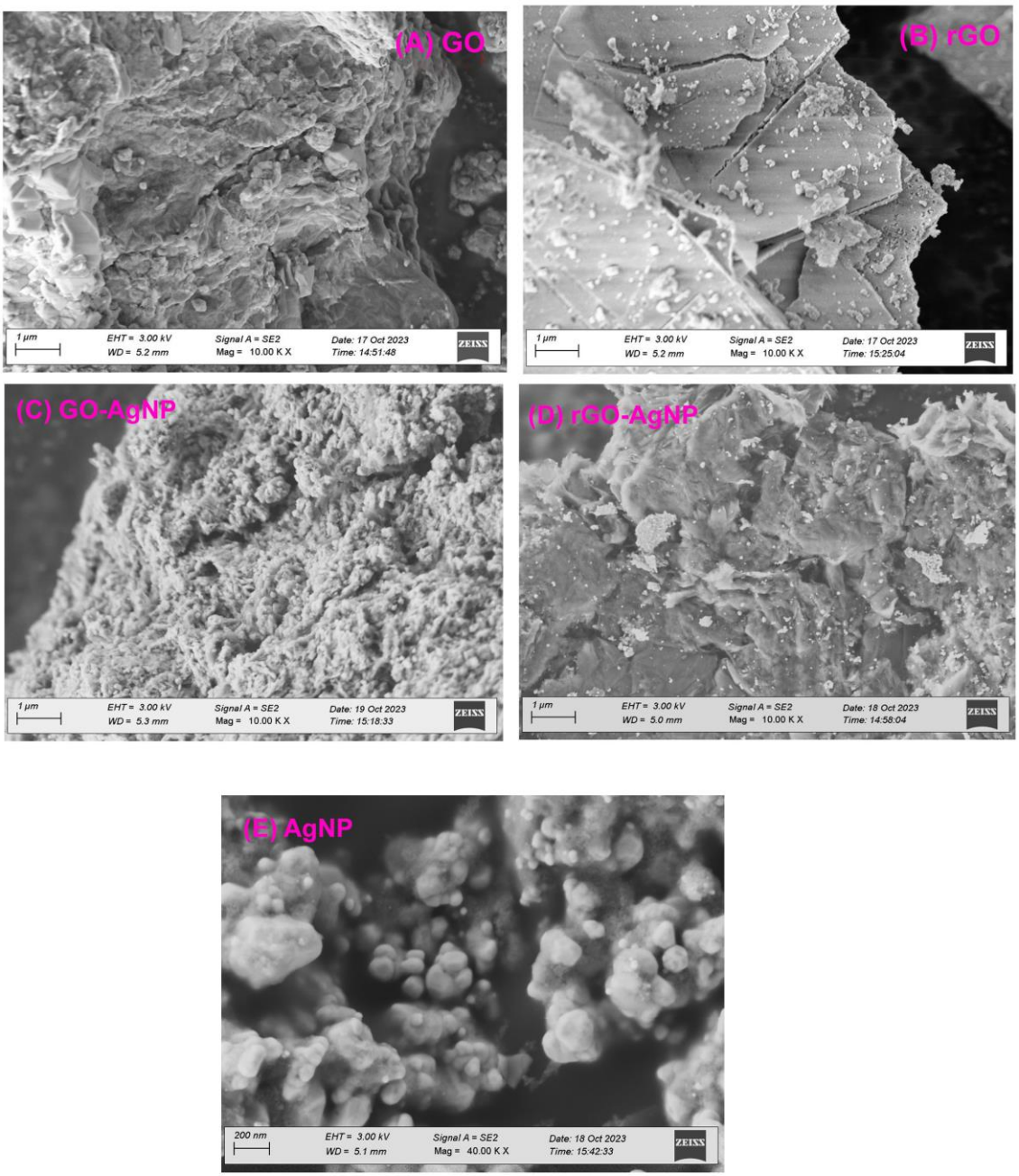

Figure 3. FE–SEM images of A. GO, B. rGO, C. GO-AgNP, D. rGO-AgNP and E. AgNP with different magnifications.

3.4. Fourier Transform Infrared Spectroscopy (FTIR) Analysis

 doi:10.20944/preprints202503.2185.v1

FTIR analysis revealed the spectra of the synthesized GO and GO-Ag nanocomposite (Figure 4), which ranged between 4000 and 500 cm^{-1}. An adsorption band corresponding to intermolecular H-bonding in GO was observed at 3437 cm^{-1}, but this band disappeared in the GO-Ag nanocomposite. In addition, bands corresponding to C−H, C−O, and C−O were observed in 2072, 1636, and 1011cm^{-1}, respectively. After doping, the intensity of the C−O and ⁻OH bands decreased, indicating that AgNPs were anchored onto the GO surface. After doping, a blue shift was observed for these peaks.

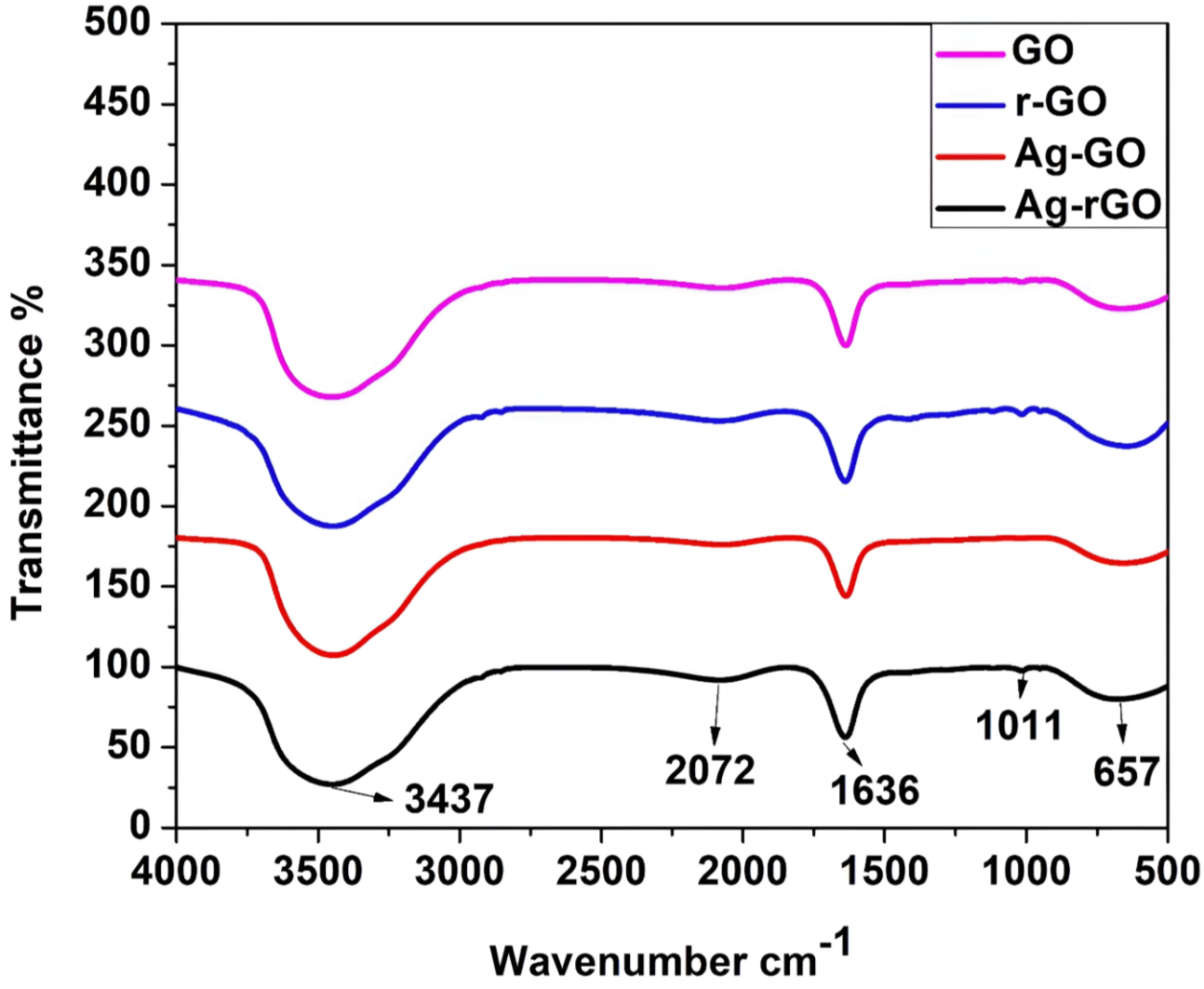

Figure 4. FTIR Spectra of GO, rGO, AgNP-GO, and AgNP-rGO composites in the wave number ranging from 500-4000 $cm^{-1.}$

3.5. Raman Spectroscopy

The Raman spectra of the GO and GO-Ag nanocomposite are shown in Figure 5. The GO showed D and G bands at 1345 and 1575 cm^{-1}, respectively, whereas the GO-Ag nanocomposite showed D and G bands at 1350 and 1590 cm^{-1}, respectively.

The attachment of hydroxyl and epoxide groups to the basal plane of carbon resulted in structural defects, which were the source of the strong D peak. The accompanying Raman spectra showed that the increased disorder of the rGO and rGO-Ag nanocomposite led to an enhancement of the D bands, while the enhanced isolated double bonds caused a broadening of the G bands of rGO and rGO-Ag. The G band of rGO-Ag nanocomposite, which can be observed in Figure 5 at 1600 cm^{-1}, was obviously shifted upward by 24 cm^{-1} compared to that of rGO (1584 cm^{-1}), which is

 doi:10.20944/preprints202503.2185.v1

consistent with previous studies that the introduction of Au resulted in a shift of the G band through electron–phonon interaction.

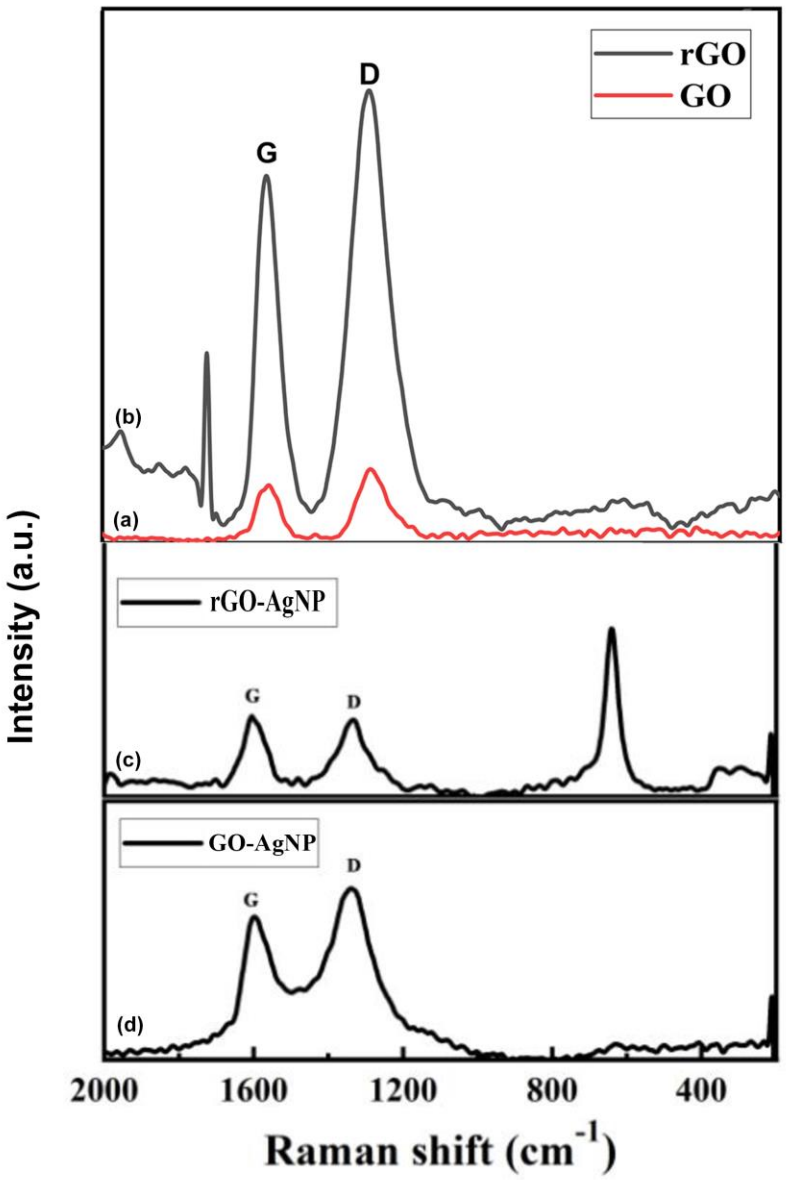

Figure 5. Raman spectra of GO, rGO, GO-AgNP and rGO-AgNP in the wave number ranging from 500-5000 cm-1.

3.6. Cell Viability Assay

Treatment of MCF-7 cells with GO nanoparticles at different concentrations (0.1, 1, 10, and 50 μM) significantly decreased the viability with increasing concentration from 1 μM and the lowest viability of 68.7% was observed in 50 μM GO. This clearly shows that GO nanoparticles induce cytotoxicity in a dose-dependent manner (Figure 6a–e). GO-AgNP treatment resulted in a 58.67% reduction in cell viability at 50 μM (Figure 6d). Treatment with rGO nanoparticles alone reduced cell

 doi:10.20944/preprints202503.2185.v1

viability by 70.1% at 50 μM (Figure 6b). Treatment with AgNPs alone reduced cell viability by 82% at 50 μM in MCF-7 cells (Figure 6c). However, the combination of rGO-AgNP treatment resulted in 65% cytotoxicity at 50 μM (Figure 6e).

When MCF-7 cells were treated with AgNPs, the viability at 10 and 50 μM was more or less the same at 84% and 82.6%, respectively. This indicates that AgNPs have a weak anticancer effect compared to GO and rGO-AgNPs (Figure 6 a–c).

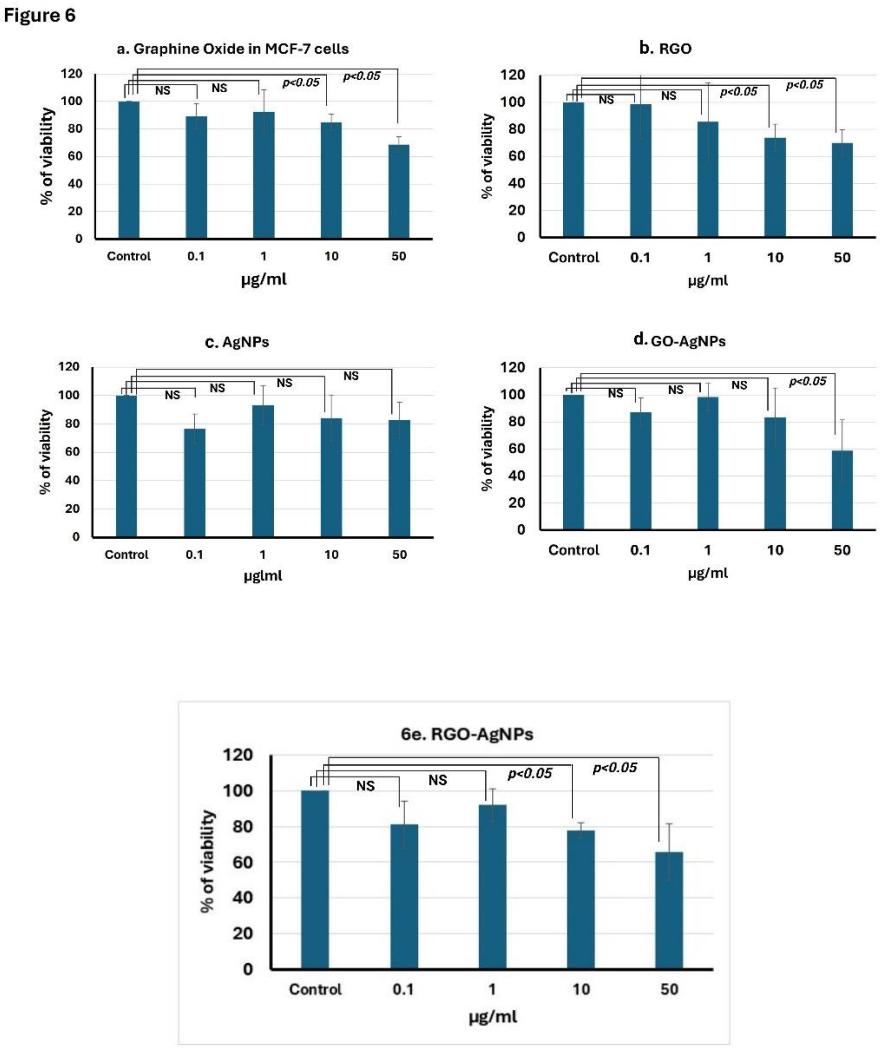

Figure 6. Nanomaterials inhibit the proliferation of MCF-7 breast cancer cells. MCF-7 were seeded in 96-well plates and treated with a. GO, b. rGO, c. AgNP, d. GO-AgNPs, and e. rGO-AgNP composites at different concentrations for 48 h. Cell viability was determined by using the MTT assay. The OD values of each treated group were compared with those of the control at the same time point. Results are shown as mean value ± SD of three independent experiments. *P<0.05* considered to be statistically significant.

3.7. Mammosphere Formation Assay

Treatment of MCF-7 cells with the nanoparticles GO, rGO, GO-AgNPs and rGO-AgNPs (10 μM) significantly reduced the mammosphere formation (Figure 7a–f). The mammosphere formation is more significantly reduced in rGO, and rGO-AgNPs treated cells when compared with GO and GO-AgNPs treated cells (Figure 7g). In addition, the spheroid size is also significantly reduced by the treatment of nanoparticles.

 doi:10.20944/preprints202503.2185.v1

Figure 7

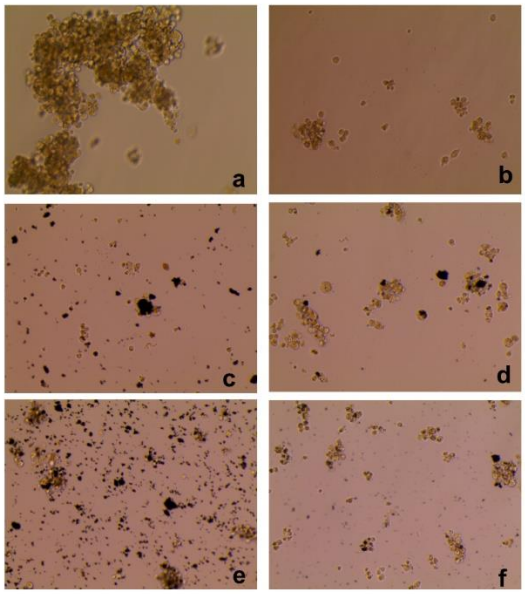

Figure 7g

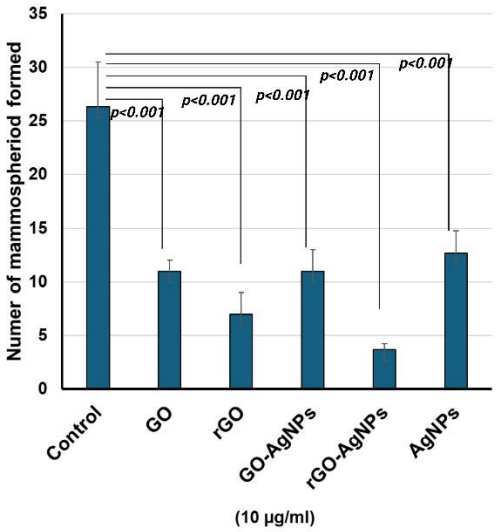

Figure 7. MCF-7 derived CSCs were allowed to form mammospheres for 7 days. A. Control, b. graphene oxide, c. reduced graphene oxide, d. GO-AgNP, e. rGO-AgNP, f. AgNPs. Treatment with nanomaterials reduced the size and number of mammospheres. Mammosphere treated with nanomaterials resulted in a lower number compared to the control, (g) Mammosphere were quantified using EVOS M5000 microscopic software. The mammosphere formation significantly reduced all the nanoparticles treatment. Mammosphere numbers more significantly reduced in rGO and rGO-AgNPs treatment. *P<0.001* considered to be more statistically significant.

3.8. Quantitative RT-PCR Analysis

Nanoparticle treatment reduced the expression of stem cell marker genes, such as *CD44*, *ALDH1A*, *SOX-2*, *NANOG*, *OCT4*, *EPCAM*, and *LAGR5* (Figure 8). The GO-AgNPs and rGO-AgNPs have most significantly inhibit the gene expression of stem cell markers when compared with other nanoparticles. However, AgNPs alone treatment did not affect gene expression of Nanog.

 doi:10.20944/preprints202503.2185.v1

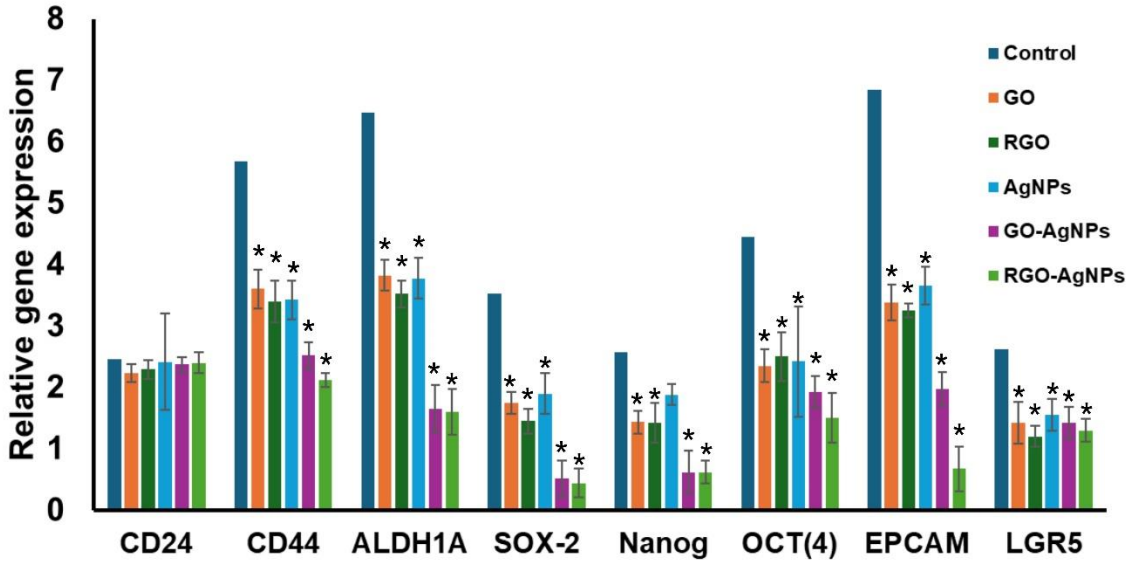

Figure 8. Treatment of MCF-7 cells with nanoparticles, significant reduction of stem cell marker gene expressions. '*' Indicates that statistically significant *(p<0.05)* reduction in gene expression when compared with control gene expression.

4. Discussion

The synthesized nanoparticles GO, rGO, and AgNPs were thoroughly characterized. The UV-Vis spectra of rGO displayed a prominent absorption band at 261 nm, reflecting the significant restoration of the conjugated sp2 carbon network. Upon deposition of AgNPs on the rGO surface, a new peak appeared at 420 nm, which corresponds to surface plasmons resonance and confirms the successful incorporation of AgNPs on to the rGO surface [53–57]. AgNPs showed a prominent diffraction peak corresponding to the (111) plane at a 2θ value of 32.152°, consistent with prior literature [58,59]. The GO-Ag nanocomposite displayed an interlayer spacing of 1.456 nm and peaks associated with both GO and AgNPs. The XRD pattern of the rGO–Ag nanocomposite revealed clear peaks corresponding to the (111) and (200) diffraction planes of face centered cubic (fcc) Ag, supporting the crystalline nature of AgNPs [54,60–62]. These results align with earlier reports describing the structural configuration of GO/AgNPs composites synthesized through the reduction of AgNO3 and GO in the presence of reducing agents [9,20,24,54,63,64]. FTIR analysis provided further confirmation of interactions within the composites. The C–N stretching vibration observed in the TAPE-reduced rGO–Ag nanocomposite produced a distinct band at 1420 cm^{-1}. Peaks at 657, 1011, 1636, 2070, and 3437 cm^{-1} were also appeared in the FTIR spectra of the rGO–Ag nanocomposite, with intensities comparatively lower than those of GO indicating the reduction process and interactions between residual hydroxyl groups and AgNPs [50,54,64,65].

Raman spectroscopy revealed that the G band, attributed to the E2g phonon of sp2 carbon atoms, and the D band, related to the breathing mode of k-point phonons with A1g symmetry, shifted upon AgNP deposition. For rGO, the G and D bands appeared at 1580 cm^{-1} and 1353cm^{-1}, respectively, suggesting structural changes and increased disorder due to AgNP intercalation [66–68]. The G band introduced the E2g phonon of the sp2 atoms of carbon, whereas the D band was attributed to the breathing mode of the k-point phonons with A1g symmetry.

The biological assessment showed that the GO-AgNPs composite demonstrated the most effective anticancer activity with the lowest cell viability of 58.67% at a concentration of 50 μM compared to GO and AgNPs alone. The enhanced antioxidant and inhibitory effects of GO-AgNPs likely disturb cellular transcriptional and translational through further experimental studies are required to elucidate the exact mechanisms [69,70]. In addition, GO, GO-AgNPs and rGO-AgNPs

 doi:10.20944/preprints202503.2185.v1

effectively inhibited MCF-7 cancer cell proliferation and mammosphere formation in which is consistent with previous studies [71,72]. Interestingly, treatment with rGO and rGO-AgNPs significantly impacted the expression of cancer stem cell associated gene expressions in breast and other types of cancers cell lines [73]. AgNPs have been induce cytotoxicity and inhibit stem cell proliferation at the transcriptional levels [74] while GO has been reported to promote the differentiation of hematopoietic stem cells [31] and myogenic progenitor cells [75].

5. Conclusions

The synthesized and characterized nanoparticles exhibit significant potential in targeting breast cancer cells and cancer stem cells. Specifically, rGO, GO-AgNPs and rGO-AgNPs demonstrated promising anticancer effects by inhibiting MCF-7 cell proliferation and mammosphere formation. These findings suggest that nanocomposites play a critical role in reducing cancer stem cell self-renewal. Further in-depth studies, including toxicity assessments and targeted drug delivery strategies, are necessary to confirm their efficacy in preclinical models of breast cancer.

Author Contributions: BV and KP conceived the idea and wrote the manuscript. KP, BV, and MS performed the experimental analysis. DT and RNM helped with data analysis. SI, JR proofread the manuscript. All authors have read and approved the final version of the manuscript.

Funding: The author(s) disclosed declare receipt of the following financial support for the research, authorship, and/or publication of this article. This work was supported in part, by the Department of Science and Technology, Science & Engineering Research Board Grant EEQ/2017/000567 to KP and by the American Heart Association Transformational Project Award 20TPA35490215 and the National Institute of Health R01 grant HL141345 to JR.

Ethical Approval: Not applicable.

Informed Consent: Not applicable.

Data Availability: The data availability statement is not applicable.

Acknowledgments: We would like to thank Mr. M. Vijayaraman for editing the manuscript. We also thank Dr. Prabhu Bhoopathy for statistical analysis.

Conflicts of Interest: The authors declare that there is no conflict of interest in the publication of this paper.

References

1. Geim, A.K. and K.S. Novoselov, *The rise of graphene.* Nat Mater, 2007. **6**(3): p. 183-91.10.1038/nmat1849.
2. Lee, C.H., et al., *Electronic structures of finite double-walled carbon nanotubes in a magnetic field.* Journal of Physics: Condensed Matter, 2008. **20**(7): p. 075213.10.1088/0953-8984/20/7/075213.
3. Novoselov, K.S., et al., *Electric field effect in atomically thin carbon films.* Science, 2004. **306**(5696): p. 666-9.10.1126/science.1102896.
4. Stoller, M.D., et al., *Graphene-based ultracapacitors.* Nano Lett, 2008. **8**(10): p. 3498-502.10.1021/nl802558y.
5. Lekshmi, G.S., et al., *Multifunctional oil-produced reduced graphene oxide - Silver oxide composites with photocatalytic, antioxidant, and antibacterial activities.* J Colloid Interface Sci, 2022. **608**(Pt 1): p. 294-305.10.1016/j.jcis.2021.08.048.
6. Khan, J.M., R. Kurchania, and V.K. Sethi, *Synthesis and characterization of two dimensional graphene lamellae based PAn nanocomposites.* Thin Solid Films, 2010. **519**(3): p. 1059-1065.https://doi.org/10.1016/j.tsf.2010.08.044.
7. Sagadevan, S., et al., *Sensor to Electronics Applications of Graphene Oxide through AZO Grafting.* Nanomaterials (Basel), 2023. **13**(5).10.3390/nano13050846.
8. Li, D., et al., *Processable aqueous dispersions of graphene nanosheets.* Nat Nanotechnol, 2008. **3**(2): p. 101-5.10.1038/nnano.2007.451.

 doi:10.20944/preprints202503.2185.v1

9. Mumtaz, M.A., et al., *Enhancing the charge transfer and redox characteristics in energy storage devices with a layered ZnNbS@graphene nanocomposite electrode material for biomedical application.* Diamond and Related Materials, 2023. **140**: p. 110519.https://doi.org/10.1016/j.diamond.2023.110519.
10. Raghavendra Babu, B., et al., *Functionalised carbon fiber based flexible symmetric supercapacitors with wider potential window for sustainable energy storage applications.* Journal of Power Sources, 2025. **625**: p. 235727.https://doi.org/10.1016/j.jpowsour.2024.235727.
11. Seonwoo, H., et al., *Reduced graphene oxide-incorporated calcium phosphate cements with pulsed electromagnetic fields for bone regeneration.* RSC Adv, 2022. **12**(9): p. 5557-5570.10.1039/d1ra05717k.
12. Li, R., et al., *Graphene oxide loaded with tumor-targeted peptide and anti-cancer drugs for cancer target therapy.* Sci Rep, 2021. **11**(1): p. 1725.10.1038/s41598-021-81218-3.
13. Croitoru, A.M., et al., *Novel Graphene Oxide/Quercetin and Graphene Oxide/Juglone Nanostructured Platforms as Effective Drug Delivery Systems with Biomedical Applications.* Nanomaterials (Basel), 2022. **12**(11).10.3390/nano12111943.
14. Sun, X., et al., *Nano-Graphene Oxide for Cellular Imaging and Drug Delivery.* Nano Res, 2008. **1**(3): p. 203-212.10.1007/s12274-008-8021-8.
15. Lu, H., et al., *MnO(2) doped graphene nanosheets for carotid body tumor combination therapy.* Nanoscale Adv, 2022. **4**(20): p. 4304-4313.10.1039/d2na00086e.
16. Sanchez, J.A., et al., *Synthesis, Characterization, and Antibacterial Activity of Graphene Oxide/Zinc Hydroxide Nanocomposites.* Applied Sciences, 2024. **14**(14): p. 6274
17. Elbasuney, S., et al., *Potential Impact of Reduced Graphene Oxide Incorporated Metal Oxide Nanocomposites as Antimicrobial, and Antibiofilm Agents Against Pathogenic Microbes: Bacterial Protein Leakage Reaction Mechanism.* Journal of Cluster Science, 2023. **34**(2): p. 823-840.10.1007/s10876-022-02255-0.
18. Hua, F., T. Yao, and Y. Yao, *Spherical Silver Nanoparticles Located on Reduced Graphene Oxide Nanocomposites as Sensitive Electrochemical Sensors for Detection of L-Cysteine.* Sensors (Basel), 2024. **24**(6).10.3390/s24061789.
19. Lu, C.H., et al., *A graphene platform for sensing biomolecules.* Angew Chem Int Ed Engl, 2009. **48**(26): p. 4785-7.10.1002/anie.200901479.
20. Sattari, S., et al., *Functionalized Graphene Platforms for Anticancer Drug Delivery.* Int J Nanomedicine, 2021. **16**: p. 5955-5980.10.2147/IJN.S249712.
21. Yaghoubi, F., et al., *A functionalized graphene oxide with improved cytocompatibility for stimuli-responsive co-delivery of curcumin and doxorubicin in cancer treatment.* Sci Rep, 2022. **12**(1): p. 1959.10.1038/s41598-022-05793-9.
22. Akhavan, O., et al., *The use of a glucose-reduced graphene oxide suspension for photothermal cancer therapy.* Journal of Materials Chemistry, 2012. **22**(27): p. 13773-13781.10.1039/C2JM31396K.
23. Fiorillo, M., et al., *Graphene oxide selectively targets cancer stem cells, across multiple tumor types: implications for non-toxic cancer treatment, via "differentiation-based nano-therapy".* Oncotarget, 2015. **6**(6): p. 3553-62.10.18632/oncotarget.3348.
24. Gurunathan, S., et al., *Green synthesis of graphene and its cytotoxic effects in human breast cancer cells.* Int J Nanomedicine, 2013. **8**: p. 1015-27.10.2147/IJN.S42047.
25. Gurunathan, S., et al., *An in vitro evaluation of graphene oxide reduced by Ganoderma spp. in human breast cancer cells (MDA-MB-231).* Int J Nanomedicine, 2014. **9**: p. 1783-97.10.2147/IJN.S57735.
26. Aparicio-Collado, J.L., et al., *Electroactive calcium-alginate/polycaprolactone/reduced graphene oxide nanohybrid hydrogels for skeletal muscle tissue engineering.* Colloids Surf B Biointerfaces, 2022. **214**: p. 112455.10.1016/j.colsurfb.2022.112455.
27. Gurunathan, S. and J.H. Kim, *Synthesis, toxicity, biocompatibility, and biomedical applications of graphene and graphene-related materials.* Int J Nanomedicine, 2016. **11**: p. 1927-45.10.2147/IJN.S105264.
28. Zhang, Y., et al., *Cytotoxicity effects of graphene and single-wall carbon nanotubes in neural phaeochromocytoma-derived PC12 cells.* ACS Nano, 2010. **4**(6): p. 3181-6.10.1021/nn1007176.
29. Li, N., et al., *The promotion of neurite sprouting and outgrowth of mouse hippocampal cells in culture by graphene substrates.* Biomaterials, 2011. **32**(35): p. 9374-82.10.1016/j.biomaterials.2011.08.065.

30. Luo, Y., et al., *Enhanced proliferation and osteogenic differentiation of mesenchymal stem cells on graphene oxide-incorporated electrospun poly(lactic-co-glycolic acid) nanofibrous mats.* ACS Appl Mater Interfaces, 2015. **7**(11): p. 6331-9.10.1021/acsami.5b00862.
31. Garcia-Alegria, E., et al., *Graphene Oxide promotes embryonic stem cell differentiation to haematopoietic lineage.* Sci Rep, 2016. **6**: p. 25917.10.1038/srep25917.
32. Stensberg, M.C., et al., *Toxicological studies on silver nanoparticles: challenges and opportunities in assessment, monitoring and imaging.* Nanomedicine (Lond), 2011. **6**(5): p. 879-98.10.2217/nnm.11.78.
33. Christopher, P. and S. Linic, *Engineering selectivity in heterogeneous catalysis: Ag nanowires as selective ethylene epoxidation catalysts.* J Am Chem Soc, 2008. **130**(34): p. 11264-5.10.1021/ja803818k.
34. Sriram, M.I., et al., *Antitumor activity of silver nanoparticles in Dalton's lymphoma ascites tumor model.* Int J Nanomedicine, 2010. **5**: p. 753-62.10.2147/IJN.S11727.
35. AshaRani, P.V., et al., *Cytotoxicity and genotoxicity of silver nanoparticles in human cells.* ACS Nano, 2009. **3**(2): p. 279-90.10.1021/nn800596w.
36. Kalishwaralal, K., et al., *Silver nano - a trove for retinal therapies.* J Control Release, 2010. **145**(2): p. 76-90.10.1016/j.jconrel.2010.03.022.
37. Liu, L., et al., *Facile synthesis of monodispersed silver nanoparticles on graphene oxide sheets with enhanced antibacterial activity.* New Journal of Chemistry, 2011. **35**(7): p. 1418-1423.10.1039/C1NJ20076C.
38. You, J.M., D. Kim, and S. Jeon, *Electrocatalytic reduction of H2O2 on thiolate graphene oxide covalently to bonded palladium nanoparticles.* J Nanosci Nanotechnol, 2012. **12**(5): p. 3943-9.10.1166/jnn.2012.6162.
39. Zhu, Y.-G., et al., *Design and synthesis of NiO nanoflakes/graphene nanocomposite as high performance electrodes of pseudocapacitor.* RSC Advances, 2013. **3**(42): p. 19409-19415.10.1039/C3RA42091D.
40. Dat, N.M., et al., *Synthesis of silver/reduced graphene oxide for antibacterial activity and catalytic reduction of organic dyes.* Synthetic Metals, 2020. **260**: p. 116260.https://doi.org/10.1016/j.synthmet.2019.116260.
41. de Luna, L.A., et al., *Comparative in vitro toxicity of a graphene oxide-silver nanocomposite and the pristine counterparts toward macrophages.* J Nanobiotechnology, 2016. **14**: p. 12.10.1186/s12951-016-0165-1.
42. Gurunathan, S. and J.H. Kim, *Graphene Oxide-Silver Nanoparticles Nanocomposite Stimulates Differentiation in Human Neuroblastoma Cancer Cells (SH-SY5Y).* Int J Mol Sci, 2017. **18**(12).10.3390/ijms18122549.
43. Nageshwaran, S., K. Majumdar, and S. Russell, *Hypergammaglobulinemia, normal serum albumin and hypercalcaemia: a case of systemic sarcoidosis with initial diagnostic confusion.* BMJ Case Rep, 2012. **2012**.10.1136/bcr.01.2012.5478.
44. Rao, V.H., et al., *A positive feedback loop between HER2 and ADAM12 in human head and neck cancer cells increases migration and invasion.* Oncogene, 2012. **31**(23): p. 2888-98.10.1038/onc.2011.460.
45. Ediriwickrema, A. and W.M. Saltzman, *Nanotherapy for Cancer: Targeting and Multifunctionality in the Future of Cancer Therapies.* ACS Biomater Sci Eng, 2015. **1**(2): p. 64-78.10.1021/ab500084g.
46. Sun, L., et al., *Smart nanoparticles for cancer therapy.* Signal Transduct Target Ther, 2023. **8**(1): p. 418.10.1038/s41392-023-01642-x.
47. Pryshchepa, O., P. Pomastowski, and B. Buszewski, *Silver nanoparticles: Synthesis, investigation techniques, and properties.* Adv Colloid Interface Sci, 2020. **284**: p. 102246.10.1016/j.cis.2020.102246.
48. Klemeyer, L., H. Park, and J. Huang, *Geometry-Dependent Thermal Reduction of Graphene Oxide Solid.* ACS Materials Letters, 2021. **3**(5): p. 511-515.10.1021/acsmaterialslett.0c00423.
49. Hassen, A., et al., *Synergistic effects of thermally reduced graphene oxide/zinc oxide composite material on microbial infection for wound healing applications.* Sci Rep, 2024. **14**(1): p. 22942.10.1038/s41598-024-73007-5.
50. Yuan, Y.G., et al., *Quercetin-mediated synthesis of graphene oxide-silver nanoparticle nanocomposites: a suitable alternative nanotherapy for neuroblastoma.* Int J Nanomedicine, 2017. **12**: p. 5819-5839.10.2147/IJN.S140605.
51. Gurunathan, S., et al., *Biocompatibility of microbially reduced graphene oxide in primary mouse embryonic fibroblast cells.* Colloids Surf B Biointerfaces, 2013. **105**: p. 58-66.10.1016/j.colsurfb.2012.12.036.
52. Kalyanaraman, A., et al., *Tamoxifen induces stem-like phenotypes and multidrug resistance by altering epigenetic regulators in ERalpha+ breast cancer cells.* Stem Cell Investig, 2020. **7**: p. 20.10.21037/sci-2020-020.
53. Elias, M., et al., *Fabrication of Ag-doped BiOF-reduced graphene oxide composites for photocatalytic elimination of organic dyes.* Heliyon, 2024. **10**(15): p. e34921.10.1016/j.heliyon.2024.e34921.

 doi:10.20944/preprints202503.2185.v1

54. Kumari, S., et al., *A Novel Synthesis of the Graphene Oxide-Silver (GO-Ag) Nanocomposite for Unique Physiochemical Applications.* ACS Omega, 2020. **5**(10): p. 5041-5047.10.1021/acsomega.9b03976.
55. Shen, J., et al., *Facile synthesis and application of Ag-chemically converted graphene nanocomposite.* Nano Research, 2010. **3**(5): p. 339-349.10.1007/s12274-010-1037-x.
56. Al-Marri, A.H., et al., *Pulicaria glutinosa extract: a toolbox to synthesize highly reduced graphene oxide-silver nanocomposites.* Int J Mol Sci, 2015. **16**(1): p. 1131-42.10.3390/ijms16011131.
57. Hu, C., et al., *Fabrication of reduced graphene oxide and sliver nanoparticle hybrids for Raman detection of absorbed folic acid: a potential cancer diagnostic probe.* ACS Appl Mater Interfaces, 2013. **5**(11): p. 4760-8.10.1021/am4000485.
58. Choi, Y.J., S. Gurunathan, and J.H. Kim, *Graphene Oxide-Silver Nanocomposite Enhances Cytotoxic and Apoptotic Potential of Salinomycin in Human Ovarian Cancer Stem Cells (OvCSCs): A Novel Approach for Cancer Therapy.* Int J Mol Sci, 2018. **19**(3).10.3390/ijms19030710.
59. Ali, M.H., et al., *Analysis of Crystallographic Structures and Properties of Silver Nanoparticles Synthesized Using PKL Extract and Nanoscale Characterization Techniques.* ACS Omega, 2023. **8**(31): p. 28133-28142.10.1021/acsomega.3c01261.
60. Priyadarsini, A., et al., *Synergistic cobalt oxide/reduced graphene oxide/biochar nano-composite catalyst: harnessing the power of the catalyst for sustainable remediation of organic dyes and chromium(vi).* RSC Adv, 2024. **14**(14): p. 10089-10103.10.1039/d4ra01031k.
61. Anaklı, D. and M. Erşan, *Optimization of reduced graphene oxide yield using response surface methodology.* Diamond and Related Materials, 2024. **148**: p. 111524.https://doi.org/10.1016/j.diamond.2024.111524.
62. C, D., et al., *Graphene-Functionalized Titanium Carbide Synthesis and Characterization and Its Cytotoxic Effect on Cancer Cell Lines.* Cureus, 2024. **16**(5): p. e61049.10.7759/cureus.61049.
63. He, Y., et al., *An overview of carbon materials for flexible electrochemical capacitors.* Nanoscale, 2013. **5**(19): p. 8799-820.10.1039/c3nr02157b.
64. Zuo, P.P., et al., *Fabrication of biocompatible and mechanically reinforced graphene oxide-chitosan nanocomposite films.* Chem Cent J, 2013. **7**(1): p. 39.10.1186/1752-153X-7-39.
65. Chook, S.W., et al., *Antibacterial performance of Ag nanoparticles and AgGO nanocomposites prepared via rapid microwave-assisted synthesis method.* Nanoscale Res Lett, 2012. **7**(1): p. 541.10.1186/1556-276X-7-541.
66. Krishnaraj, C., et al., *Green synthesis of Ag and Au NPs decorated rGO nanocomposite for high impedimetric electrochemical sensor as well as enhanced antimicrobial performance against foodborne pathogens.* Arabian Journal of Chemistry, 2024. **17**(1): p. 105379.https://doi.org/10.1016/j.arabjc.2023.105379.
67. Yuan, X., et al., *Functionalized graphene oxide-based carbon paste electrode for potentiometric detection of copper ion(ii).* Analytical Methods, 2012. **4**(10): p. 3332-3337.10.1039/C2AY25674F.
68. Giovanni, M., et al., *Noble metal (Pd, Ru, Rh, Pt, Au, Ag) doped graphene hybrids for electrocatalysis.* Nanoscale, 2012. **4**(16): p. 5002-5008.10.1039/C2NR31077E.
69. Yuan, Y.G., et al., *Graphene Oxide-Silver Nanoparticle Nanocomposites Induce Oxidative Stress and Aberrant Methylation in Caprine Fetal Fibroblast Cells.* Cells, 2021. **10**(3).10.3390/cells10030682.
70. Sadiq, H., et al., *Assessment of antioxidant activity of pure graphene oxide (GO) and composite V2O5/GO using DPPH radical and H2O2 scavenging assays.* Journal of Sol-Gel Science and Technology, 2023. **108**(3): p. 840-849.10.1007/s10971-023-06231-6.
71. Kaur, R., et al., *Silver nanoparticles induces apoptosis of cancer stem cells in head and neck cancer.* Toxicol Rep, 2024. **12**: p. 10-17.10.1016/j.toxrep.2023.11.008.
72. Dasari, N., G.S. Guntuku, and S. Pindiprolu, *Targeting triple negative breast cancer stem cells using nanocarriers.* Discov Nano, 2024. **19**(1): p. 41.10.1186/s11671-024-03985-y.
73. Rajanahalli, P., C.J. Stucke, and Y. Hong, *The effects of silver nanoparticles on mouse embryonic stem cell self-renewal and proliferation.* Toxicol Rep, 2015. **2**: p. 758-764.10.1016/j.toxrep.2015.05.005.

 doi:10.20944/preprints202503.2185.v1

74. Gao, X., et al., *Transcriptomic and proteomic responses of silver nanoparticles in hepatocyte-like cells derived from human induced pluripotent stem cells.* Toxicol In Vitro, 2022. **79**: p. 105274.10.1016/j.tiv.2021.105274.
75. Wierzbicki, M., et al., *Graphene Oxide Scaffold Stimulates Differentiation and Proangiogenic Activities of Myogenic Progenitor Cells.* Int J Mol Sci, 2020. **21**(11).10.3390/ijms21114173.